Journal of Materials Chemistry C

Accepted Manuscript

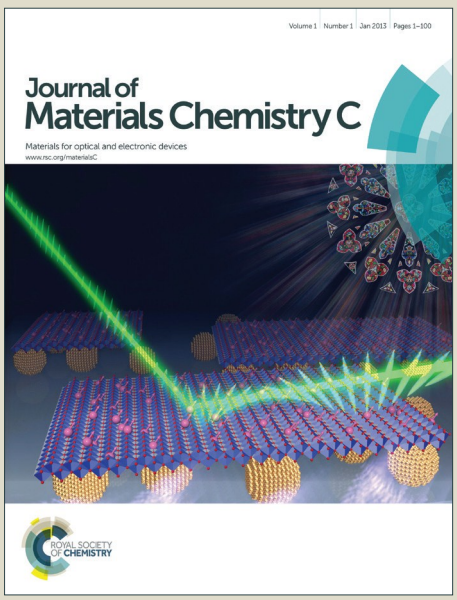

ROYAL SOCIETY OF CHEMISTRY

www.rsc.org/materialsC

Journal of Materials Chemistry C

ARTICLE

The shift of optical absorption band edge of ZnO/ZnS core/shell nanotube arrays beyond quantum effects

[l]Received 00th January 20xx,
Accepted 00th January 20xx

DOI: 10.1039/x0xx00000x

www.rsc.org/

Samar Tarish,[‡a, b] Ahmed Al-Haddad,[‡a, b] Rui Xu,[‡a] Dawei Cao,[a] Zhijie Wang,*[a, c] Shengchun Qu[c], Ghulam Nabi,[a] Yong Lei*[a]

Unlike conventional investigations that focus on the manipulation of optical absorption band edge for a single componential material through quantum confinement effects, in this paper, we study the optical absorption property of well-ordered ZnO/ZnS core/shell nanotube arrays. Our data point out that the profile of the absorbance spectrum of ZnO/ZnS nanotube arrays is determined by the two components and geometrical parameters of the nanostructure arrays. We find that both of the ZnO and ZnS show a decrease in optical band gap with the increase of ZnS thickness and the diameter of nanotube arrays, which is interestingly out of explanation from the material aspect. The subsequent finite-difference-time-domain simulations support such observations and illustrate that the geometrical and periodical parameters could also impact the optical absorption of the core/shell nanostructure arrays, even without concerning the quantum effects.

Introduction

Photon absorption capability is a key factor that determines the efficiency of solar energy conversion devices and the detectivity of optical sensors. The central component in these devices is a semiconductor that behaves as both a photon absorber and a signal converter. Thus, tremendous attention has been concentrated on the optical property of semiconductors.[1,2] Once the semiconductor is fixed, it is hard to modulate the absorption onset which is governed by the band gap of the corresponding semiconductor. One of the popular methods to tune the absorption properties of a semiconductor is to reduce the size to a characteristic value like exciton Bohr radius. In this case, the band gap becomes larger as compared with the relevant bulk material followed by a blue shift of the optical absorption onset, attributing to the localization of electrons and holes in a confined space and thereby resulting in observable quantization of the energy levels of the electrons.[3,4] Attempts focusing on the impact of the geometrical parameters of nanostructure arrays with multiple components on the absorption profiles beyond quantum effects, however, are rarely reported, owing to the difficulty in obtaining and manipulating well-ordered multi-componential nanostructure arrays.

Recently, techniques based on anodic aluminum oxide (AAO) template turn out to be one type of the most popular methodologies for preparing perfectly ordered nanostructure arrays, due to the unique advantages in low-cost fabrication, easy scalability and high manipulation.[5-8] A large series of nanostructure arrays including nanodot arrays, nanowire arrays, nanotube arrays, and nanocone arrays, has been realized. By controlling the preparation of the different components sequentially, multi-componential nanostructure arrays could also be highly producible.[9,10]
Concerning the fact that the ZnO/ZnS core/shell nanostructure is one of the most studied structures applied widely in optical sensors, biosensors, and solar cells.[11-13] In the present paper, we focus on the tunablity of optical band gap of well-ordered ZnO/ZnS core/shell nanotube arrays. By modulating the ZnS shell with different thicknesses, we found that absorption band edge of the structure presented a red shift when we increased the thickness of ZnS. To be exciting, more careful analyses on the Tauc plots indicated that not only the optical band gap of ZnS became smaller, the band gap of ZnO also shifted to a lower value, with the increase in the diameter of the nanotube. Subsequent finite difference time domain (FDTD) simulations confirmed such observations from theoretical aspects and revealed that geometrical parameters of the nanostructure arrays could impact the absorption profile without the consideration of quantum effects. Thus, this paper provides a new perspective to look at the shift of absorption onset for composite semiconductors.

[a] Institute for Physics and IMN MacroNano, Ilmenau University of Technology, Professor Schmidt Strasse 26, 98693 Ilmenau, Germany. *Email: yong.lei@tu-ilmenau.de
[b] Department of Physics, College of Science, University of Al-Mustansiriyah, Baghdad, Iraq.
[c] Key Laboratory of Semiconductor Materials Science, Institute of Semiconductors, CAS, Beijing 100083 , P. R. China. *Email: wangzj@semi.ac.cn
† Electronic Supplementary Information (ESI) available: [details of any supplementary information available should be included here]. See DOI: 10.1039/x0xx00000x
‡ These authors contributed equally to this work.

RESULTS AND DISCUSSION:

Representative top and cross-sectional views of scanning electron microscopic (SEM) images of the prepared AAO template are shown in Fig. S1a ESI†, in which an array of well-ordered alumina pores could be clearly observed. The pores present an average diameter around 70 nm, a pore distance of 110 nm and a thickness of 1800 nm, offering a good platform for the subsequent formation of ZnO nanotube arrays. As exhibited in Fig. 1a and Fig. S1b ESI†, the ZnO nanotube array prepared by a typical atomic layer deposition (ALD) procedure on AAO template has a uniform thickness and profile, through which we could investigate the optical property precisely by adjusting the geometrical and compositional parameters. Fig. 1 b-e show the SEM images of the targeting ZnO/ZnS nanotube arrays, which were synthesized by soaking the ZnO/AAO nanotube arrays in sodium sulfide solution to remove the AAO template and form the ZnS shells synchronously. With the prolonging of sulfidation time, the diameter and thickness of the nanotubes increase accordingly. These free-standing nanotubes present a well-ordered distribution and a uniform profile, giving rise to a stable optical property. Thus we can focus more deeply on the association of the optical performance with the geometric and compositional parameters. Such ZnO/ZnS core/shell nanostructure arrays were synthesized by following our reported procedures.[14]

To provide more information about the material characterization, X-ray photoelectron spectroscopy (XPS) was measured and the whole XPS spectra of ZnO and ZnO/ZnS nanotube arrays for the sample prepared at 50 min sulfidation time are shown in Fig. 2a, where the standard XPS spectrum from ZnO single crystal is also given for reference. With regard to the ZnO/ZnS sample, concomitant sulfur peaks like $S2p_{3/2}$(162.4 eV), $S2p_{1/2}$(162.8 eV) and SLMM could be clearly found in the yellow curves, indicative of the formation of ZnS shell on the ZnO nanotube array, these XPS results are in good agreement with the reports.[15,16] Resolved spectra for the $Zn2p_{3/2}$ peak are shown in Fig. 2b and all these three samples have the same peak. The $Zn2p_{3/2}$ peak obtained from the ZnO nanotubes appears to be symmetric with its peak at 1022.3 eV, which is a little larger than the value of Zn in bulk ZnO. The peaks of $Zn2p_{1/2}$ from the three samples given in Fig. S2 ESI† also show a similar feature. For the ZnO/ZnS, the sulfur peak is found at 162.2 eV binding energy (Fig. 2c), which is in the typical energy range for sulfides. The oxygen peaks O1s for ZnO shown in Fig. 2d consists of two components which are related to different chemical bonds at the surface. The one at 530.9 eV binding energy is related to Zn-O bond while the one at 532.3 eV is linked to the absorbate.[17,18] To be noticed, for the ZnO/ZnS sample, the peak of Zn-O bond disappears, thereby confirming the existence of fully covered ZnS shell.

In order to adjust the geometric parameters of the core/shell nanostructure, the immersing time in sodium sulfide solution was selected as 30, 40, 50 and 60 min, respectively. Fig. 3a shows the representative TEM images of the relevant nanotubes. With the increase of soaking time, the diameter of the tubes increases accordingly and a thin outer layer appears, indicating the formation of ZnS shell, which also presents an increasing feature with the prolonging of the reaction time, though the thickness of ZnO shows a slightly decaying feature.

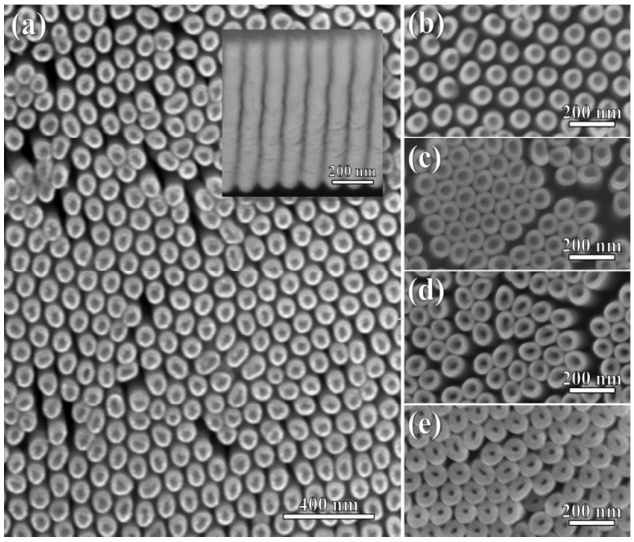

Fig. 1 SEM images (a) Top view of ZnO nanotube arrays after removing AAO template, inset shows cross-sectional view. (b-e) ZnO/ZnS nanotube arrays after sulfidation for (30, 40, 50 and 60 min), respectively.

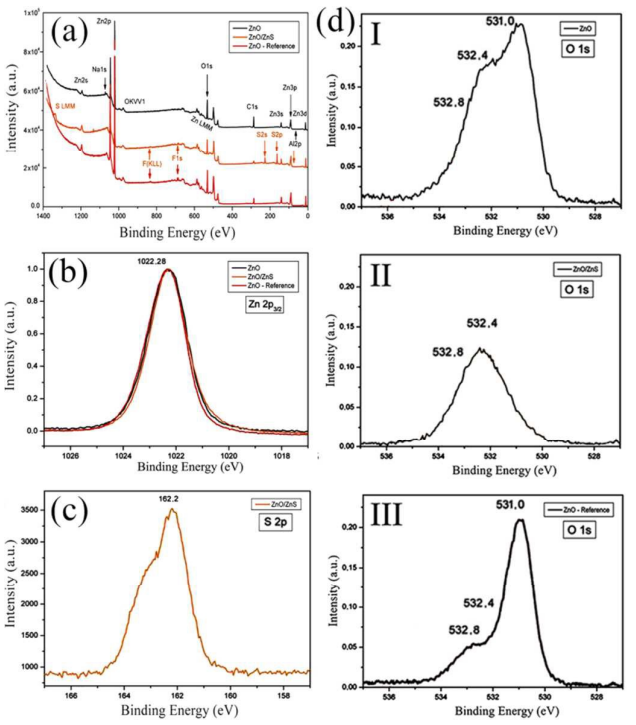

Fig. 2 XPS spectra of the ZnO and ZnO/ZnS nanotube arrays: (a) Overview scan, (b) $Zn2p_{3/2}$, (c) S2p and (d) O1s peaks.

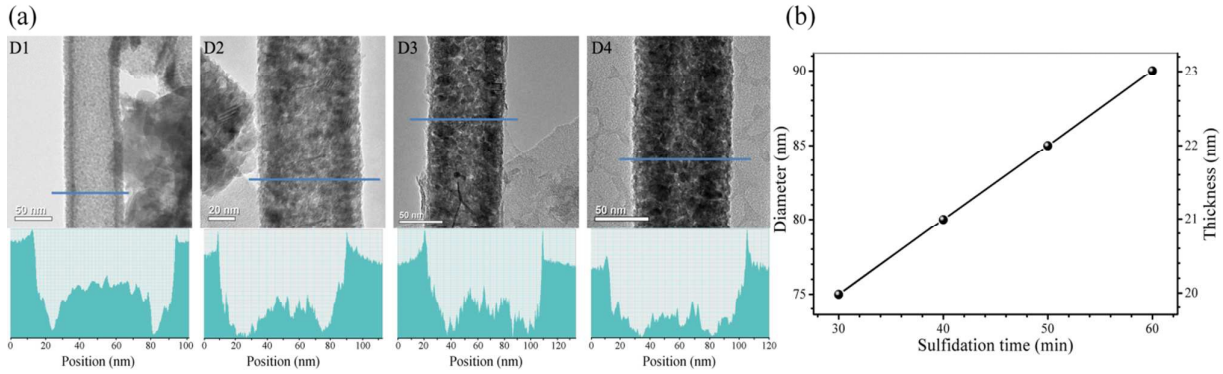

Fig. 3 Structural characterization of ZnO/ZnS nanotube array: (a) low magnification TEM micrograph of a single ZnO/ZnS nanotube that experienced sulfidation process for D1=30 min, D2=40 min, D3=50 min and D4=60 min, respectively. The below is the intensity profile perpendicular to the centre axis of the nanotube. (b) The linear relationships between the sulfidation time and both of the outer diameter and the total wall thickness of the structure.

This could be more directly confirmed by the TEM-EDX line scan in Fig. S3 ESI†. The more detailed information about the dependence of the diameter and thickness of the nanotubes on sulfidation time is given in Fig. 3b. As the time is increased from 30 min to 60 min, the diameter and thickness could be manipulated from 75-90 nm and 20-23 nm, respectively. These controllable geometric parameters give a chance to tune the according optical parameters precisely.

Fig. 4a presents the absorbance spectra of the series of nanotube arrays, which were measured by the transmittance mode. The transmittance spectra of the corresponding nanotube arrays are given in Fig. S4a ESI†. Both of these optical spectra show a distinct red shift for the sample with long sulfurization time. Since ZnS has a larger band gap than ZnO, it is surprising to observe such red shift for the optical onset. It seems that the increase of the ZnS shell makes the band gap smaller, which is hard to explain from material aspect. To confirm such observation from theory, FDTD simulation was performed using the same geometric parameters obtained from TEM images for the series of ZnO/ZnS nanotube arrays and the resulting absorbance and transmittance spectra are given in Fig. 4b and Fig. S4b ESI†, respectively. To be noted, these simulated spectra exhibit the same tendency of red shift as that in the experimental spectra, thereby supporting the observation.

In order to investigate such phenomenon deeply, Tauc plots were converted from the experimental absorbance spectra. As shown in Fig. 4c, all of these plots exhibit two obvious linear parts. One is corresponding to ZnO and the other one is from ZnS. By calculating the intercept of these linear parts to the X axis, band gap values for ZnO and ZnS, which are in agreement with the reported values,[19,20] could be attained. Fig. 4d presents these values in accordance with the diameters of the nanotube arrays. In consistency with the absorbance analysis, both ZnO part and ZnS part present a decrease in band gap with the increase of the nanotube diameter. ZnO has a slightly decrease in band gap from 3.28 eV to 3.26 eV when the diameter is increasing from 75 nm to 90 nm. However, ZnS presents a larger range of reduction in band gap from 3.58 eV to 3.30 eV. This indicates that the band gap of the shell material is more sensitive to the diameter of nanotube array than that of the core material.

To support such interesting observation, we also calculated the Tauc plots for the simulated data (Fig. S4c ESI†) and the dependence of band gap value on the diameter of nanotube array is plotted in Fig. 4e. Though the band gap values of ZnO and ZnS show somewhat variations due to the slight mismatch in geometric features of the real samples with the ideal ones, both ZnO and ZnS exhibit a decrease of band gap with the increase of the diameter, and the band gap of ZnO is less sensitive towards the diameter change than that of ZnS, in good agreement with the experimental results. Moreover, the sensitivity of band gap to the thickness of the nanotubes shows the same tendency. To quantify the band gap sensitivities towards the dimension variations, we plot the curves of $\triangle Eg/Eg$ vs T/D (thickness/diameter) for the experimental and simulated results, as shown in Fig. 4f and g. The higher decaying rate of $\triangle Eg/Eg$ of ZnS over ZnO indicates the larger sensitivity of band gap for ZnS over ZnO.

The band gap values above are calculated based on direct band gap transition. Considering that the materials may show a band gap transition change in nanoscale, we also calculate the band gap values based on indirect transition model and the according results are given in Fig. S5 ESI†. Though the band gap values show some variations by comparing with those calculated by the direct model, the resulting band gap values present the same decreasing feature with the increase of the diameter and thickness of the nanotubes. To test the limit of band gap shift, we perform a further simulation by increasing the thickness of ZnS until the gaps of between the nanostructures are filled. To be noted, the band gap values of both ZnS and ZnO always present a decreasing feature with the increase in the thickness of nanotubes in the whole investigating range, as presented in Fig. S6 ESI†.

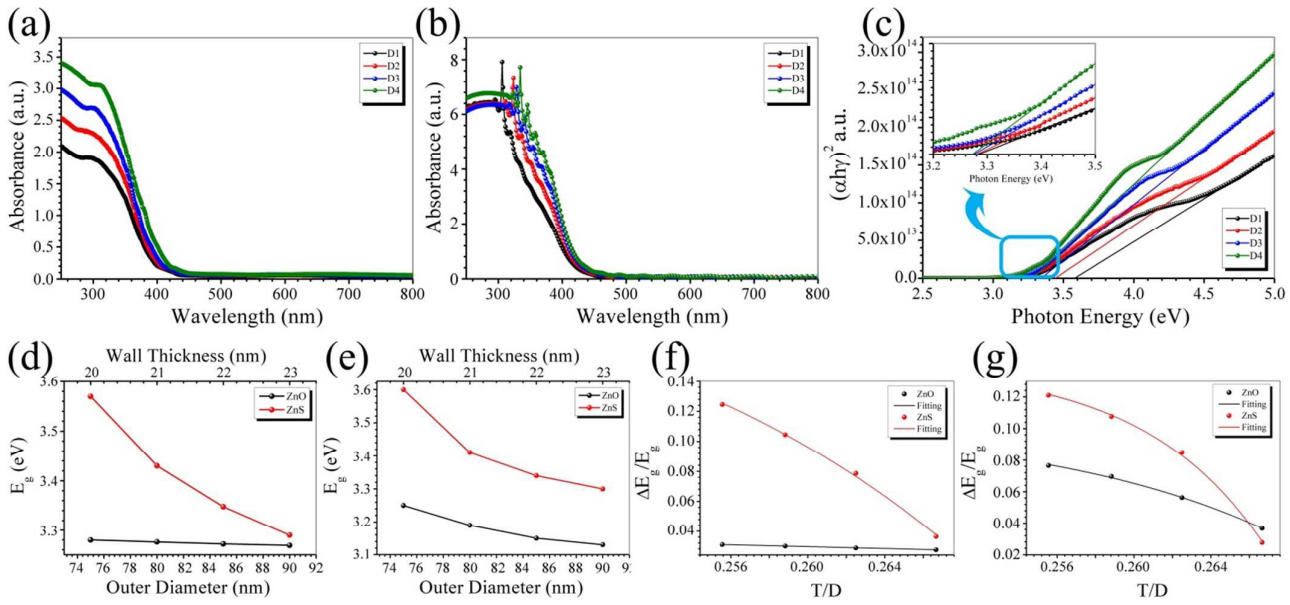

Fig. 4 (a) Experimental absorbance spectra of the prepared ZnO/ZnS nanotube arrays. (b) Simulated absorbance spectra of the proposed ZnO/ZnS nanotube arrays using FDTD simulation. (c) Tauc plots of direct optical band gap calculations from experimental results. (d, e) Optical band gap of the ZnO/ZnS nanotube array as a function of diameter and wall thickness for experimental and simulated results, respectively. (f, g) Plots of ΔEg/Eg vs. T/D for experimental and FDTD simulated results, respectively.

All these results mean that such phenomenon is from the compositional and geometric feature of the nanostructure arrays. Compositional feature governs the main location of optical onset and geometric characteristic determines the shift. As a renowned factor to cause the shift of band gap, the quantum effect has been studied most, which becomes influential only when the dimensions of the nanostructure are smaller than the Bohr radius of the corresponding material.[1] Herein, quantum effect could be ruled out, since the thicknesses of ZnO and ZnS layers are all larger than the Bohr radius of ZnO and ZnS.[21,22] The only reason to cause such band gap shift could be from the specific interactions of the incident radiations with the periodic nanostructures.

To investigate it more, electric field distribution around the nanostructure arrays under the illumination of photons at 300 nm was simulated by the FDTD software.[23] Fig.5a shows FDTD simulation of the electric field intensity profiles of one hexagonal array of nanotubes for the employed samples with different ZnS shell thicknesses (D1, D2, D3 and D4) under illumination of 300 nm. The electric field distributions under other illuminations, like 200 nm, 400 nm and 500 nm, are given in Fig S7 ESI†. As shown in Fig. 5a, the field intensity is the highest at the surface of nanotubes and decays as the spot moves from the surface to the void space, suggesting that interaction of the radiation with the periodic nanostructure happens mainly on the outer surface of the nanotube, where the photons can be absorbed in the highest possibility. By comparing the samples with different diameters, we find that the field intensity at the surface of nanotube shows an increasing feature when the diameter is enlarged and the spacing between the nanotubes becomes smaller. This implies a stronger coupling of the electric field for the samples with a narrower spacing, thereby resulting a higher absorption efficiency of photons and a redshift of absorbance threshold. To be noted, such redshift is irrelevant to the intrinsic properties of the material and only attributed to the morphological features. Considering that the electric field at the shell surface has a higher value than that around the ZnO core and the higher value is more susceptible to the dimension variations, it is understandable to observe a larger sensitivity of band gap of ZnS shell than ZnO core to the increase of the diameter of the nanotube.

The results give a good agreement with the simulation report using self-consistent charge density functional tight binding method,[24] where the band gap of ZnO/ZnS decreases with increasing shell thickness if the thickness of the core is fixed. In order to analyse the electric field intensities more deeply, the curves of the near-field intensity enhancement $|E/E_0|$ at the nanotube surface in accordance with geometric parameters of the nanotubes are shown in Fig. 5b, where E/E_0 is the component of the local electromagnetic field parallel to the incident direction. After passing through the array, the light propagates over a few microns inside the structure, where the photonic structure performance can be quantitatively characterized by calculating the $|E/E_0|$ intensity along the vertical line and through the centre of the structure.[25]

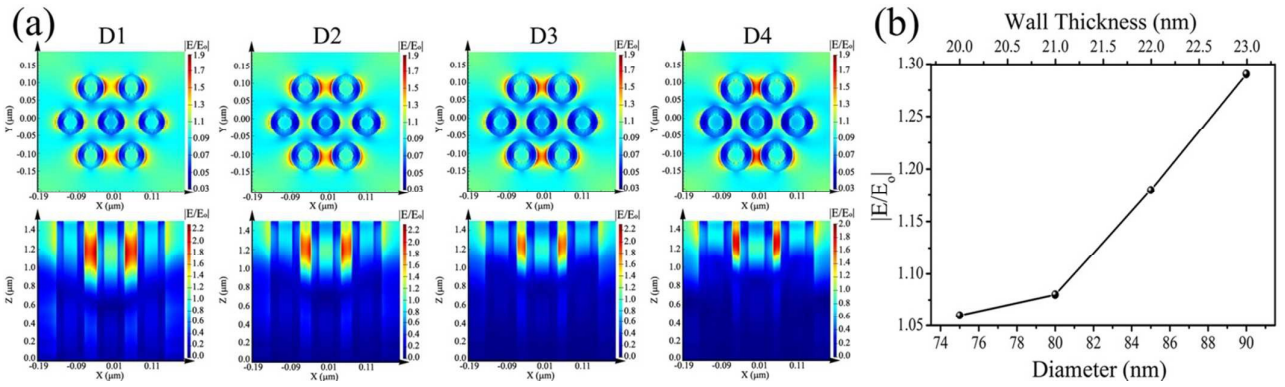

Fig. 5 (a) FDTD simulation of E-field amplitude distribution under 300 nm illumination showing top and cross-sectional views of D1, D2, D3 and D4; the relevant results of other samples are given in Fig. S7 ESI†. (b) FDTD calculated $|E/E_o|$ enhancement at the top surface of ZnO/ZnS nanotube array as a function of outer diameter and wall thickness of ZnO/ZnS nanotube array under 300 nm illumination.

The $|E/E_o|$ displays an arising feature with the increase of the wall thickness and diameter, supporting that the geometric parameters could indeed impact the absorbance onset of the periodic nanostructures, through modulating the interactions of the incident radiations with the ordered nanostructure arrays, rather than via the well-known quantum effects. To be noted, the outer material is more sensitive in the optical band gap shift towards the dimensional changes of the ordered nanostructure arrays, in comparison with the inner material. This implies that this phenomenon is surface-related, like the well-known surface plasmon resonance effect in metallic nanostructures, though the electron density in our structures is low.

Conclusions

For the first time, we have investigated the shift of optical band gap for ZnO/ZnS nanotube arrays from both experimental and simulating aspects, and we observed that both the band gaps of ZnO and ZnS in nanostructural hybrids became smaller when the thickness and diameter of the nanotube arrays were tuned larger. This phenomenon is not governed by the renowned quantum effect but by the interaction of the incident radiations with the periodic nanostructures, which greatly expands our understanding about the optical properties of semiconductors. The corresponding tunability enables the nanostructure arrays with a great potential in the application of optical sensors and photoelectronics.

EXPERIMENTAL SECTION:

The ZnO nanotube arrays on anodic aluminum oxide (AAO) templates were grown by a PicoSun ALD system according to the following procedure. Diethylzinc (Zn $(C_2H)_2$, DEZ) and H_2O were selected as the precursors. After the reaction chamber was heated to 250 °C, the DEZ precursor was pulsed for 0.1 s and purged for 5 s, followed by a 0.1 s pulse and 5 s purge of H_2O. This procedure was repeated for 250 to 300 cycles according to the desired wall thickness of ZnO nanotubes. After ZnO deposition, all the AAO nanopores were covered with ZnO. To expose the top surface of the ZnO/AAO nanotubes, an ion beam etching (Gatan, Inc, Model 682) was used for 10 min. Then to obtain ZnS-coated ZnO nanotubes, the ZnO/AAO nanotube samples were immersed in 0.01 M sodium sulfide (Na_2S) (98% Aldrich) solution at 60 °C. The reaction time was controlled to modulate the ZnS shell thickness. After being taken out from the solution and washed with deionized water, the samples were dried at the 50 °C under vacuum conditions for 1 h.[14]

Three-dimensional Finite-difference time-domain (FDTD) simulations were carried out by using the program FDTD Solutions (version 8.9) from Lumerical Solutions, Inc. In order to maintain the accuracy and stability of the FDTD calculations, the smallest grid size to accurately model the set system without being computationally prohibitive was obtained in an iterative fashion (convergence testing). In our implementation of FDTD, convergence testing was done by starting the first calculation with a grid size of $\lambda_o/20$, where λ_o is the smallest wavelength expected in the simulation, and then decreasing the grid size by half in sequential simulations and comparing the results of the calculations.

Surface morphological analysis of the products was carried out on a scanning electron microscope SEM (Hitachi S-4800). The optical absorption was measured by a UV–vis spectrometer (Cary 5000 UV–vis-NIR). The XPS spectra were measured with an energy resolution of <0.6 eV/step, a pass energy of 15 eV, the number of scans of 10 times (Axis Ultra DLD system from Shimadzu). For the crystal structure characterization, TEM (Libra 200 FE) was used.

Acknowledgements

The authors kindly acknowledge the help from Dr. Henry Romanus for TEM measurements, the help from Stephanie Reiß, Marcel Himmerlich and Prof. Dr. Stefan Krischok for the

XPS measurments. Acknowledgment is made to Institute of Micro-Nanotechnology Center (ZMN). This work is financially supported by the European Research Council (ThreeDsurface, Grant 240144), BMBF (ZIK-3DNanoDevice, Grant 03Z1MN11), German Research Foundation (DFG: LE 2249_4-1), and DAAD-Deutscher Akademischer Austauschdienst. Dr. Dawei Cao sincerely thanks the support from the Alexander von Humboldt Foundation.

References

1 A. Al-Haddad, Z. Wang, R. Xu, H. Qi, R. Vellacheri, U. Kaiser and Y. Lei, *J. Phys. Chem. C*, 2015, **119**, 16331–16337.
2 Y. W. and N. Herron, *J. Phys. Chem.*, 1987, **91**, 5005–5008.
3 S. Yang, D. Prendergast and J. B. Neaton, *Nano Lett.*, 2010, **10**, 3156–3162.
4 L. C. Venema, J. W. G. Wildoer, J. W. Janssen, S. J. Tans, H. L. J. T. Tuinstra, L. P. Kouwenhoven and C. Dekker, *Science*, 1999, **283**, 1011–1013
5 A. Al-Haddad, Z. Zhan, C. Wang, S. Tarish, R. Vellacheria and Y. Lei, *ACS Nano*, 2015, **9**, 8584–8591.
6 L. Liang, Y. Xu, C. Wang, L. Wen, Y. Fang, Y. Mi, M. Zhou, H. Zhao and Y. Lei, *Energy Environ. Sci.*, 2015, **8**, 2954–2962.
7 L. Shi, Y. Xu and Q. Li, *Nanoscale*, 2010, **2**, 2104–2108.
8 Y. Zheng, W. Wang, Q. Fu, M. Wu, K. Shayan, K. M. Wong, S. Singh, A. Schober, P. Schaaf and Y. Lei, *Chempluschem*, 2014, **79**, 1622–1630.
9 L. Wen, Z. Wang, Y. Mi, R. Xu, S. H. Yu and Y. Lei, *Small*, 2015, **11**, 3408-3428.
10 Z. Wang, D. Cao, R. Xu, S. Qu, Z. Wang and Y. Lei, *Nano Energy*, 2016, **19**, 328-362.
11 X. Fang, Y. Bando, U. K. Gautam, T. Zhai, H. Zeng, X. Xu, M. Liao and D. Golberg, *Crit. Rev. Solid State Mater. Sci.*, 2009, **34**, 190–223
12 A. K. Giri, C. Charan, A. Saha, V. K. Shahi and A. B. Panda, *J. Mater. Chem. A*, 2014, **2**, 16997–17004.
13 J. Schrier, D. O. Demchenko, L. Wang and a P. Alivisatos, *Nano Lett.*, 2007, **7**, 2377–2382.
14 S. Tarish, Z. Wang, A. Al-Haddad, C. Wang, A. Ispas, H. Romanus, P. Schaaf and Y. *Lei*, *J. Phys. Chem. C*, 2015, **119**, 1575–1582.
15 H. Ma, J. Han, Y. Fu, Y. Song, C. Yu and X. Dong, *Appl. Catal. B*, 2011, **102**, 417-423.
16 P. Chen, L. Gu and X. Cao, *CrystEngComm*, 2010, **12**, 3950-3958.
17 A. I. Martin-Concepción, F. Yubero, J. P. Espinos, J. Garcia-Lopez and S. Tougaard, *Surf. Interface Anal.*, 2003, **35**, 984–990.
18 J. V. Lauritsen, S. Porsgaard, M. K. Rasmussen, M. C. R. Jensen, R. Bechstein, K. Meinander, B. S. Clausen, S. Helveg, R. Wahl, G. Kresse and F. Besenbacher, *ACS Nano*, 2011, **5**, 5987–5994
19 X. Gao, J. Wang, J. Yu and H. Xu, *CrystEngComm*, 2015, **17**, 6328–6337.
20 J. Kennedy, P. P. Murmu, P. S. Gupta, D. A. Carder, S. V. Chong, J. Leveneur and S. Rubanov, *Mater. Sci. Semicond. Process.*, 2014, **26**, 561–566.
21 J. C. Johnson, H. Q. Yan, P. D. Yang and R. J. Saykally, *J. Phys. Chem. B*, 2003, **107**, 8816–8828.
22 H. Tang, G. Xu, L. Weng, L. Pan and L. Wang, *Acta Mater.*, 2004, **52**, 1489-1494.
23 J. Zhao, A. O. Pinchuk, J. M. Mcmahon, S. Li, L. K. Ausman, A. L. Atkinson and G. C. Schatz, *Acc. Chem. Res.*, 2008, **41**, 1710–1720.
24 S. Saha, S. Sarkar, S. Pal and P. Sarkar, *J. Phys. Chem. C*, 2013, **117**, 15890–15900.
25 B. M. Wong and A. M. Morales, *J. Phys. D. Appl. Phys.*, 2009, **42**, 055111–055116.

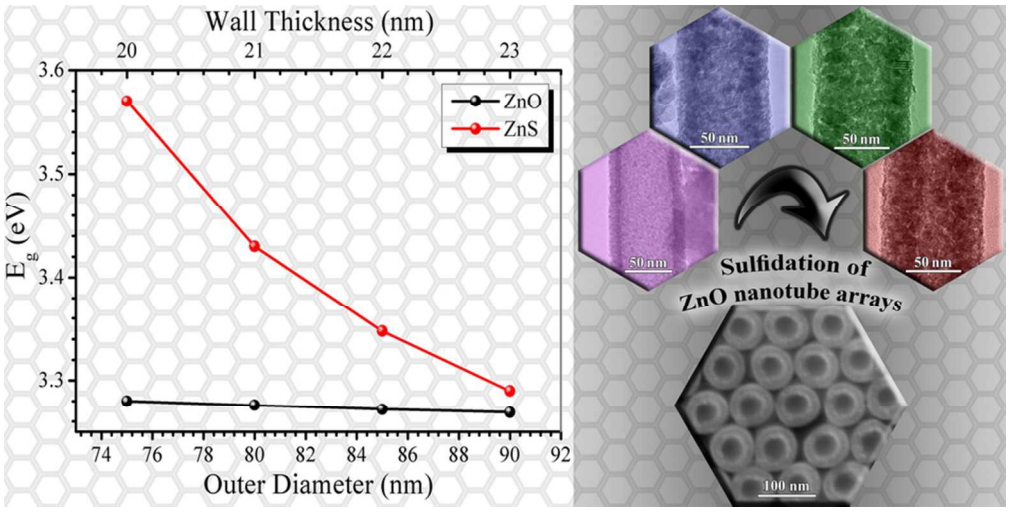

80x40mm (300 x 300 DPI)